Exploring machine learning for predicting elastic buckling and ultimate moments of steel decks in bending

Vitaliy V. Degtyarev[1]

Abstract

Accurate predictions of the elastic buckling and ultimate moments of steel decks in bending are essential for obtaining economic and safe designs. The existing design methods give accurate results for some deck profiles while producing unsafe or overly conservative predictions for others. This paper explores machine learning in the form of the Support Vector Machine regression (SVR) for estimating the elastic buckling and ultimate moments of steel decks. Eight SVR models for predicting the following properties of North American steel deck profiles were developed: plate buckling coefficient of stiffened flanges, plate buckling coefficient of unstiffened flanges, plate buckling coefficient for distortional buckling of deck flanges with a longitudinal stiffener, local elastic buckling moment of stiffened flanges, local elastic buckling moment of unstiffened flanges, distortional elastic buckling moment of a web-edge flange junction, distortional elastic buckling moment of a flange-stiffener junction, and ultimate moment. The dataset used for the model training, validation, and testing consisted of 1152 finite element simulations performed on deck models previously validated on experimental data. The developed SVR models demonstrated a good generalization ability and excellent prediction accuracy, which exceeded the accuracy of the existing design methods. The SVR models were interpreted by evaluating feature importance and feature effects using the SHapley Additive exPlanations (SHAP) method. The obtained feature importance and feature effects aligned well with the mechanics-based knowledge, confirming the abilities of the SVR models to capture and reveal the underlying physics from the data used for the model development. A web application for predicting steel deck properties in bending by the developed SVR models was created and deployed to the cloud. It can be opened and run in a browser on any device, including mobile. The application's source code, which was made available on GitHub, can be used to run the application on a local machine.

1. Introduction

Corrugated cold-formed steel (CFS) roof and floor decks have been used in construction worldwide. Steel decks are available in many different shapes and offer several benefits, including a high strength-to-weight ratio, the economy in transportation and handling, and fast and easy installation. The structural design of steel decks is governed by national standards, which generally

---

[1] Design and Research Engineer, New Millennium Building Systems, <vitaliy.degtyarev@newmill.com>, <vitdegtyarev@yahoo.com>

recognize the Effective Width Method (EWM) and the Direct Strength Method (DSM) (AISI S100-16, AS/NZS 4600:2018).

The EWM developed by von Karman et al. (1932) and Winter (1947) considers a part of a thin plate ineffective in resisting compression load due to the plate local buckling. The effective width is determined by replacing a non-uniform stress distribution in a thin plate after buckling with the equivalent rectangular stress distribution. The EWM considers the cross-section elements separately, not accounting for their interactions, and requires multiple iterations to determine CFS members' section properties. Being based on the concept of local buckling, the EWM does not explicitly consider distortional buckling, which may result in unconservative predictions for the distortional buckling failures (Yu and Lokie 2006). Steel deck profiles often fail in local buckling of stiffened and unstiffened deck flanges. Still, they may also exhibit distortional buckling of flange-longitudinal stiffener junctions or web-edge flange junctions when unstiffened edge flanges are in compression. It was previously shown that the EWM might provide unconservative predictions of the deck strength governed by distortional buckling (Degtyarev 2020a).

In the DSM (Schafer and Peköz 1998, Schafer 2008, Schafer 2019), the CFS member strength is a function of buckling loads determined from the elastic buckling analysis of the entire cross-section. The DSM allows for predicting the CFS member strength governed by distortional buckling and the strength of the members optimized by multiple stiffeners, which the EWM cannot easily achieve. Despite its many benefits, the DSM demonstrated overly conservative strength predictions for flexural members with slender compression elements (Schafer and Peköz 1998, Schafer 2008), especially when the cross-sections are not symmetric with respect to the bending axis (Dudenbostel and Sputo 2016, Raebel and Gwozdz 2018, Raebel et al. 2020, Oey and Papangelis 2020, Degtyarev 2020a). Steel deck manufacturers offer profiles with non-symmetric cross-sections and slender compression elements. The DSM underpredicts the flexural strength of such profiles, which is undesirable and slows down the DSM adoption by the steel deck industry.

Advanced finite element analysis (FEA), which is capable of accurate predictions of the deck strength in bending (Degtyarev 2020a, 2020b, 2020c, and 2020d), can be used as an alternative to the EWM and the DSM. However, it requires advanced software, modeling expertise, and substantial computational resources, which are not always available to designers. Even when the resources are available and designers possess the required skills, computationally intensive FEA is not always practical in design.

This study explores the applicability of emerging machine learning (ML) methods to the steel deck design, which may provide accuracy comparable with FEA at a low computational cost. ML is a branch of artificial intelligence (AI) and computer science that builds predictive models based on available data. ML has been successfully applied to many structural engineering problems (Çevik et al. 2015, Salehi and Burgueño 2018, Sun et al. 2021), including CFS structures. Artificial neural networks (ANNs) were employed for predicting the available rotation capacity of CFS beams (D'Aniello et al. 2014, Ali 2017), distortional buckling stress of cold-formed steel members (Pala 2006, Pala and Caglar 2007), web crippling strength of cold-formed steel decks (Guzelbey et al. 2006), shear buckling coefficient of CFS channels with large holes in the web (Pham 2018), shear elastic buckling load and ultimate shear strength of CFS channels with staggered web perforations (Degtyarev 2021b, 2021c, Naser et al. 2021, Degtyarev and Naser 2021), design load of CFS

compression members (El-Kassas et al. 2002), and uplift capacity of metal roof panels (Sirca Jr. and Adeli 2001). ANNs were also used for the optimization of CFS beams by Adeli and Karim (1997) and Karim and Adeli (1999) and for predicting the strength and deflections of strengthened CFS profiles by Taheri et al. (2021). Fang et al. (2021a, 2021b, 2021c) employed a deep belief network to predict the web crippling strength and axial capacity of CFS members. Genetic programming was applied to formulate the distortional buckling stress of C-sections in compression (Pala 2008) and for the optimal design of CFS columns (Lee et al. 2006).

The accuracy of ML models in the reviewed studies exceeded the accuracy of the existing design methods and descriptive equations, which makes the use of ML methods for estimating the elastic buckling and ultimate moments of steel decks in bending promising. In this study, Support Vector Machine regression (SVR) models for predicting the following deck properties were trained and optimized using an extensive database of FEA results: 1) plate buckling coefficient of stiffened flanges, $k_{l,stiff}$; 2) plate buckling coefficient of unstiffened flanges, $k_{l,unstiff}$; 3) plate buckling coefficient for distortional buckling of deck flanges with a longitudinal stiffener, $k_{d,flange}$; 4) local elastic buckling moment of stiffened flanges, $M_{crl,stiff}$; 5) local elastic buckling moment of unstiffened flanges, $M_{crl,unstiff}$; 6) distortional elastic buckling moment of a web-edge flange junction, $M_{crd,web}$; 7) distortional elastic buckling moment of a flange-stiffener junction, $M_{crd,flange}$; and 8) ultimate moment, M_u. The developed SVR models were interpreted by obtaining and analyzing partial feature importance and feature effects using the SHapley Additive exPlanations (SHAP) method. The SVR models demonstrated an excellent prediction accuracy, which considerably exceeded the accuracy of the traditional CFS design methods. A web application based on the developed SVR models was created and made publicly available.

2. Data Acquisition
The data required to develop the ML models were obtained from the FEA of North American steel deck profiles shown in Fig. 1 and Table 1. The following steel thicknesses were considered: 0.45 mm (26 GA), 0.60 mm (24 GA), 0.75 mm (22 GA), and 0.91 mm (20 GA) for 1F and 0.75 mm (22 GA), 0.91 mm (20 GA), 1.20 mm (18 GA), and 1.52 mm (16 GA) for all other profiles. Four steel yield strengths of 228, 276, 345, and 414 MPa were evaluated. The decks were analyzed in the positive (top flanges in compression) and negative (bottom flanges in compression) bending, which are also referred to as the normal and inverted bending orientations (BO), respectively.

The FEA results of some deck profiles presented in Fig. 1 and Table 1 were previously published in Degtyarev (2020a). In this study, 960 additional FE simulations were conducted to cover wider ranges of deck variables. The combined database (Degtyarev 2021a) consists of 1408 samples and includes the deck with the following span lengths: 914, 1219, and 1524 mm for 1F; 1219, 1829, and 2438 mm for 1.5B, 1.5BST1, 1.5BST2, and 1.5BST3; 1829, 2438, and 3048 mm for 2CST1, 2CST2, and 2CST3; and 3048, 3658, and 4267 mm for 3N, 3CST1, 3CST2, and 3CST3.

The deck was modeled in ANSYS with four-node structural shell elements, SHELL181. The material properties were described by an elastic modulus of 2.03×10^5 MPa, a Poisson's ratio of 0.3, and nonlinear stress-strain diagrams proposed by Gardner and Yun (2018), with true stresses and strains determined per Appendix C.6 of EN 1993-1-5:2006. The models were discretized with quadrilateral elements with maximum sizes of 5 and 10 mm in the directions across and along the deck span, respectively.
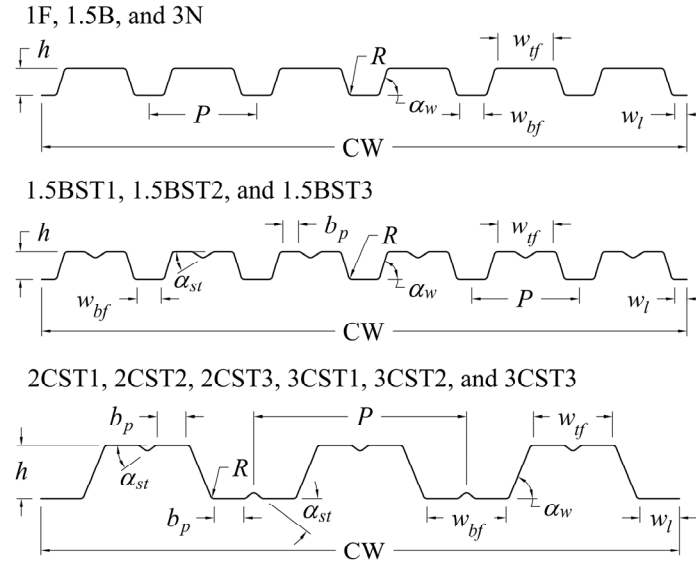
Figure 1: Dimensional Parameters of Deck Profiles

Table 1: Dimensions of Deck Profiles

Deck	h (mm)	P (mm)	w_{tf} (mm)	w_{bf} (mm)	w_l (mm)	α_w (deg)	R (mm)	b_p (mm)	α_{st} (deg)	Number of Hats	CW (mm)
1F	25	94	20.0	20.0	8.4	46.4	3.2	–	–	9	840
1.5B	38	155	79.9	35	17.5	72.5	4.8	–	–	6	928
3N	77	204	127	39.7	19.1	83.0	4.8	–	–	3	612
1.5BST1	38	155	79.9	35	17.5	72.5	4.8	22.7	30.6	6	928
1.5BST2	38	155	79.9	35	17.5	72.5	4.8	31.8	30.6	6	928
1.5BST3	38	155	79.9	35	17.5	72.5	4.8	27.2	30.6	6	928
2CST1	53	307	121.0	121.0	60.5	64.1	4.8	43.3	30.6	3	920
2CST2	53	307	121.0	121.0	60.5	64.1	4.8	52.4	30.6	3	920
2CST3	53	307	121.0	121.0	60.5	64.1	4.8	34.3	30.6	3	920
3CST1	77	307	114.3	114.3	57.2	67.4	4.8	42.8	36.5	3	920
3CST2	77	307	114.3	114.3	57.2	67.4	4.8	50.3	36.5	3	920
3CST3	77	307	114.3	114.3	57.2	67.4	4.8	35.4	36.5	3	920

Fig. 2 shows the boundary conditions of the deck models. They consist of the symmetry degree-of-freedom constraints at the deck mid-span nodes, vertical translation restraints of the top flange nodes at the support, lateral displacement restraint of one node at the deck bottom flange edge to prevent rigid body motion, and coupled vertical displacements of deck bottom flange nodes at the load location. The models were loaded by a vertical force applied to the primary node of the coupled set at $L/3$ from the support (where L is the deck span). More details on the FE models can be found in Degtyarev (2020a).

Elastic buckling and nonlinear static analyses of the deck models were performed. The obtained elastic buckling modes were classified as local buckling of stiffened flanges, local buckling of unstiffened flanges, distortional buckling of a flange-stiffener junction, or distortional buckling of a web-edge flange junction, as shown in Fig. 3. The loads and bending moments corresponding to these buckling modes were determined and stored.
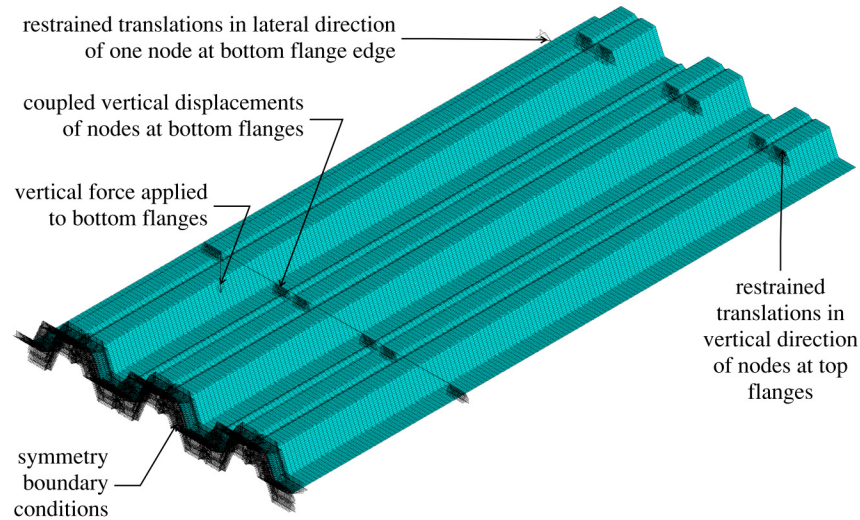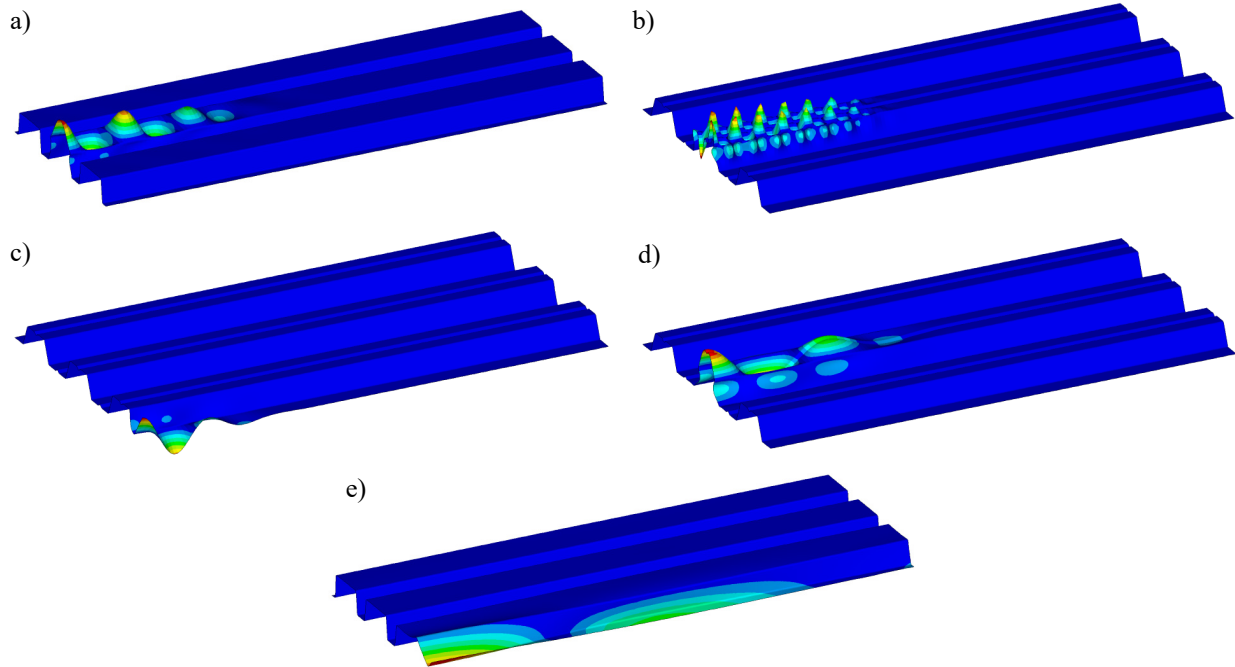
4

Figure 2: Boundary Conditions of FE Deck Models

Figure 3: Typical Deck Buckling Modes
a) Local buckling of a flange stiffened by webs; b) Local buckling of a flange stiffened by a web and a longitudinal stiffener; c) Local buckling of an unstiffened flange; d) Distortional buckling of a flange-stiffener junction; e) Distortional buckling of a web-edge flange junction

The ultimate moments were determined from the nonlinear static analysis, which followed the elastic buckling analysis. Initial geometric imperfections, as well as material and geometric nonlinearities, were considered. The initial geometric imperfections with the magnitude of 1/150 of the compression flange width were specified based on the first elastic buckling mode obtained from the elastic buckling analysis. The FE models of the deck were validated against physical test results in Degtyarev (2020a, 2020c).

3. Dataset

The database of the FE simulation results (Degtyarev 2021a) includes 224 samples for the deck profiles with the elastic-perfectly plastic and bilinear steel constitutive models. The previous study showed that the elastic-perfectly plastic, bilinear, and nonlinear stress-strain relationships resulted in similar ultimate moments (Degtyarev 2020a). Therefore, the 224 results were excluded from the dataset, ensuring that each considered combination of the deck variables is represented by one dataset sample with the nonlinear material law. The database also includes 32 results for modified 1.5B and 3N decks, designated as 1.5BR and 3NR in the previous study. These profiles were excluded from the dataset because they are not conventional decks available on the market. Thus, the $M_{crl,stiff}$, $k_{l,stiff}$, and M_u dataset used in this study included 1152 samples. For the considered deck profiles, local buckling of an unstiffened flange and distortional buckling of a web-edge flange junction can only occur for decks in the negative bending. Therefore, the $M_{crl,unstiff}$, $k_{l,unstiff}$, and $M_{crd,web}$ dataset included 576 samples. The distortional buckling of a flange-stiffener junction, described by $M_{crd,flange}$ and $k_{d,flange}$, was represented by 720 samples.

Fig. 4 shows distributions of the dataset variables, including span length, L; deck height, h; deck thickness, t; deck web angle, α_w; bend radius at the sheet steel centerline, r; out-to-out widths of the top and bottom flanges at the centerline, b_{tfo} and b_{bfo}, respectively; out-to-out width of the lip (unstiffened edge flange) at the centerline, b_{lo}; flange stiffener angle, α_{st}; out-to-out stiffener height, h_{sto}; the number of deck hats, N_{hats}; deck pitch, P; steel yield stress, F_y; the deck bending orientation; $M_{crl,stiff}$; $M_{crl,unstiff}$; $M_{crd,web}$; $M_{crd,flange}$; M_u; $k_{l,stiff}$; $k_{l,unstiff}$; and $k_{d,flange}$. The out-to-out widths of the flanges (b_{tfo}, b_{bfo}, and b_{lo}) were used in the models instead of the flat widths because the out-to-out widths are usually reported by the deck manufacturers. The α_{st} and h_{sto} values of the decks without intermediate longitudinal flange stiffeners were taken as 0. Ranges of the independent variables in the dataset were as follows: 914 mm $\leq L \leq$ 4267 mm, 25 mm $\leq h \leq$ 77 mm, 0.45 mm $\leq t \leq$ 1.52 mm, 46° $\leq \alpha_w \leq$ 83°, 3.4 mm $\leq r \leq$ 5.5 mm, 23 mm $\leq b_{tfo} \leq$ 137 mm, 23 mm $\leq b_{bfo} \leq$ 128 mm, 10 mm $\leq b_{lo} \leq$ 64 mm, 0° $\leq \alpha_{st} \leq$ 36.5°, 0 mm $\leq h_{sto} \leq$ 15 mm, 3 $\leq N_{hats} \leq$ 9, 93 mm $\leq P \leq$ 308 mm, and 228 MPa $\leq F_y \leq$ 414 MPa.

Two observations about the plate buckling coefficients of stiffened and unstiffened flanges, with values of 4.00 and 0.43 specified in AISI S100-16, can be made from Fig. 4. The dataset $k_{l,stiff}$ values between 3.29 and 5.08 reflect the web contribution, which resulted in either a reduction of $k_{l,stiff}$ below the theoretical value of 4.00 for a plate simply supported on four sides, or an increase of the buckling coefficient above the theoretical value depending on the profile geometry. The obtained $k_{l,unstiff}$ values were higher than the theoretical value of 0.43 and ranged between 0.55 and 8.17. The unexpectedly high $k_{l,unstiff}$ values, which exceeded the $k_{l,stiff}$ values for some profiles, can be explained as follows. The theoretical $k_{l,unstiff}$ value of 0.43 was determined assuming an infinitely long plate buckled in a single half-wave mode (Timoshenko and Gere 1963). In this study, the unstiffened deck flanges had large but finite aspect ratios and exhibited multiple half-wave buckling modes (see Fig. 3c), producing high buckling coefficients. The deck webs connected to the unstiffened flanges also contributed to the obtained $k_{l,unstiff}$ values.
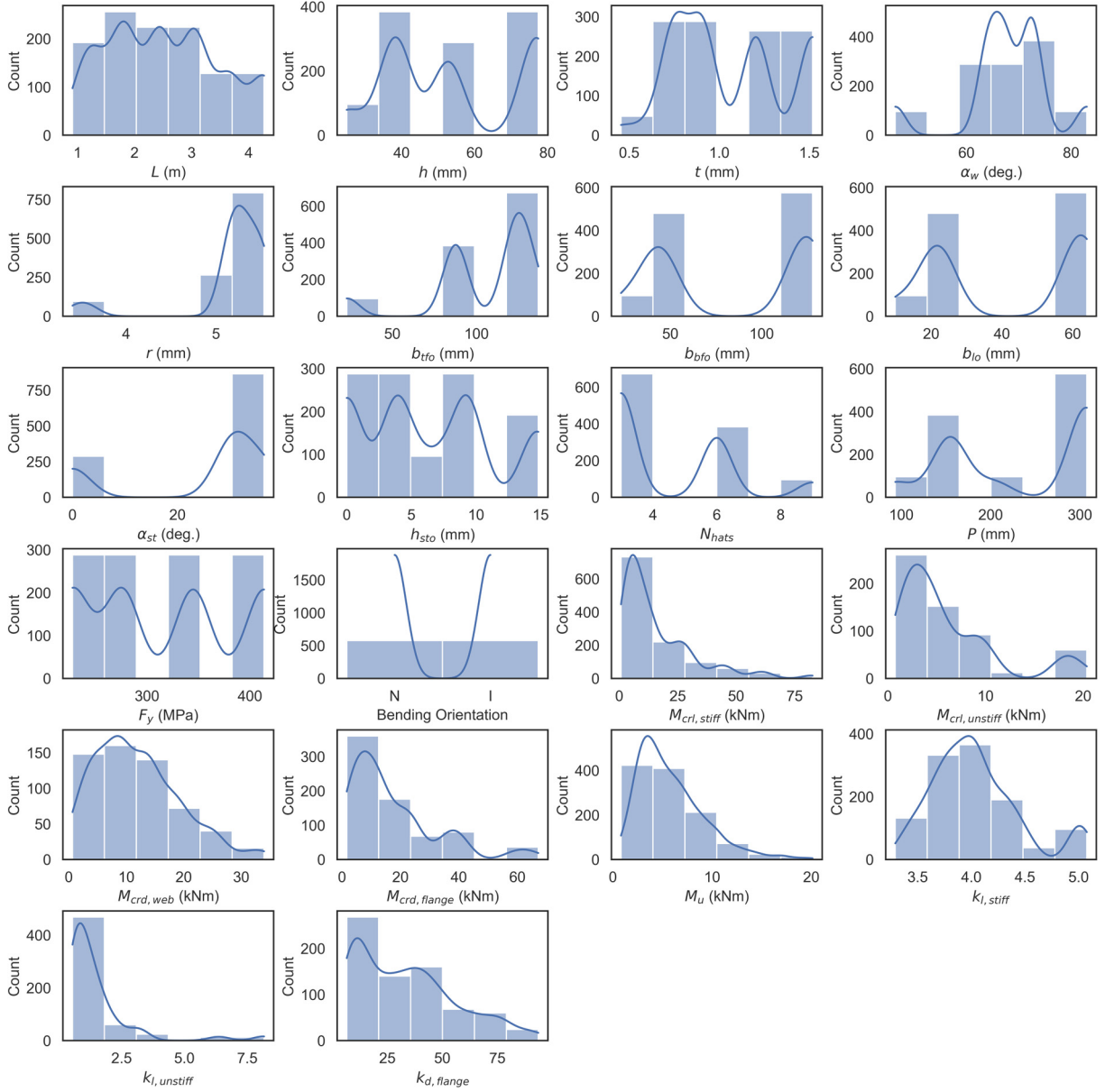
Figure 4: Distributions of Dataset Variables

4. Support Vector Machine Regression

Predictive models for the deck properties in bending were developed using the ε-SVR algorithm proposed by Vapnik and his colleagues (Vapnik 1995, Cortes and Vapnik 1995, Vapnik et al. 1997, Smola and Schölkopf 2004). SVR is a supervised ML algorithm that seeks a hyperplane function with the maximum ε deviation from the targets and the minimum flatness. The hyperplane $\pm \varepsilon$ defines decision boundaries insensitive to ε. The "soft margin" constant, C, is introduced to account for outliers, which often exist in practical applications and impede finding a hyperplane that approximates the data with ε precision. The "soft margin" constant determines the compromise between the hyperplane flatness and the prediction errors. Kernel functions are used in the ε-SVR algorithm to handle nonlinear data. They transform the original data to high-dimensional kernel space where a linear hyperplane function can be found. Several hyperparameters must be specified

before model training, including the kernel function type and its parameters, the "soft margin" constant, and the tolerance margin ε. The advantages of SVR compared with other ML regression algorithms consist of the high efficiency of handling high-dimensional data with balancing the model complexity and prediction error, insensibility to outliers, ability to handle nonlinear data, good generalization ability, and no need for large amounts of data.

The SVR algorithm was implemented in a Python-based open-source ML library *scikit-learn* (Pedregosa et al. 2011). Eight separate models for predicting $k_{l,stiff}$, $k_{l,unstiff}$; $k_{d,flange}$, $M_{crl,stiff}$, $M_{crl,unstiff}$, $M_{crd,web}$, $M_{crd,flange}$, and M_u were created and optimized. The input variables of the models included L, h, t, α_w, r, b_{tfo}, b_{bfo}, b_{lo}, α_{st}, h_{sto}, N_{hats}, P, F_y (in the M_u model only), and the deck bending orientation (in the $k_{l,stiff}$, $k_{d,flange}$, $M_{crl,stiff}$, $M_{crd,flange}$, and M_u models only; 1 and 2 were used for the normal and inverted bending orientations, respectively). An extensive hyperparameter search was performed using an open-source Python-based library *Optunity* (Claesen et al. 2014) with particle swarm optimization (Clerc and Kennedy 2002).

The SVR models were validated and tested using the ten-fold cross-validation method, where the dataset is randomly split into training and test data in a specified proportion. In this study, 80% of the data were assigned to the training/validation set and 20% to the test set. The training data is divided into ten groups, nine of which are used for model training, and the remaining one is used for model validation. The training/validation process is repeated ten times, with each group serving as the validation set. The final evaluation of the model performance is done on the test data, which the model did not see during training.

Each input parameter value in the training set was standardized using Eq. (1) to make scales of the parameters uniform, which helps the algorithm train more efficiently.
$$x' = (x - \mu)/\sigma \tag{1}$$
where x' is the standardized value of the input variable, x is the original (non-standardized) value of the variable, μ and σ are the mean and standard deviation of the variable's original values. The test set input values were also standardized using the μ and σ values obtained for the training set.

The model performances were assessed with the following performance metrics commonly used in ML (Naser and Alavi 2020): root-mean-square-error (RMSE), mean absolute error (MAE), mean percentage error (MAPE), determination coefficient (R^2), the minimum, maximum, mean, and coefficient of variation values of the FEA-to-SVR ratios.
$$RMSE = \sqrt{\frac{1}{n}\sum_{i=1}^{n}(y-x)^2} \tag{2}$$
$$MAE = \frac{1}{n}\sum_{i=1}^{n}|y-x| \tag{3}$$
$$MAPE = \frac{100}{n}\sum_{i=1}^{n}\left|\frac{y-x}{y}\right| \tag{4}$$
$$R^2 = 1 - \frac{\sum_{i=1}^{n}(y-x)^2}{\sum_{i=1}^{n}(y-\mathrm{x})^2} \tag{5}$$
where n is the number of samples, y is the target value from FEA, and x is the target value predicted by SVR.

The determined optimal hyperparameters for the SVR models are given in Table 2. The radial basis function (RBF) was specified for all models.

Table 2: Optimal Hyperparameters of SVR Models

Hyperparameter	Predicted Property							
	$k_{l,stiff}$	$k_{l,unstiff}$	$k_{d,flange}$	$M_{crl,stiff}$	$M_{crl,unstiff}$	$M_{crd,web}$	$M_{crd,flange}$	M_u
C	5931	5309	1582	9977	9380	5311	1572	3880
γ	0.018	0.124	0.251	0.099	0.139	0.249	0.043	0.068
ε	0.032	0.010	0.067	0.035	0.049	0.048	0.009	0.053

5. Performance of SVR Models

The prediction performance of the developed SVR models on training and test sets is presented in Fig. 5. Performance metrics for buckling coefficients and bending moments are shown in Tables 3 and 4, respectively.
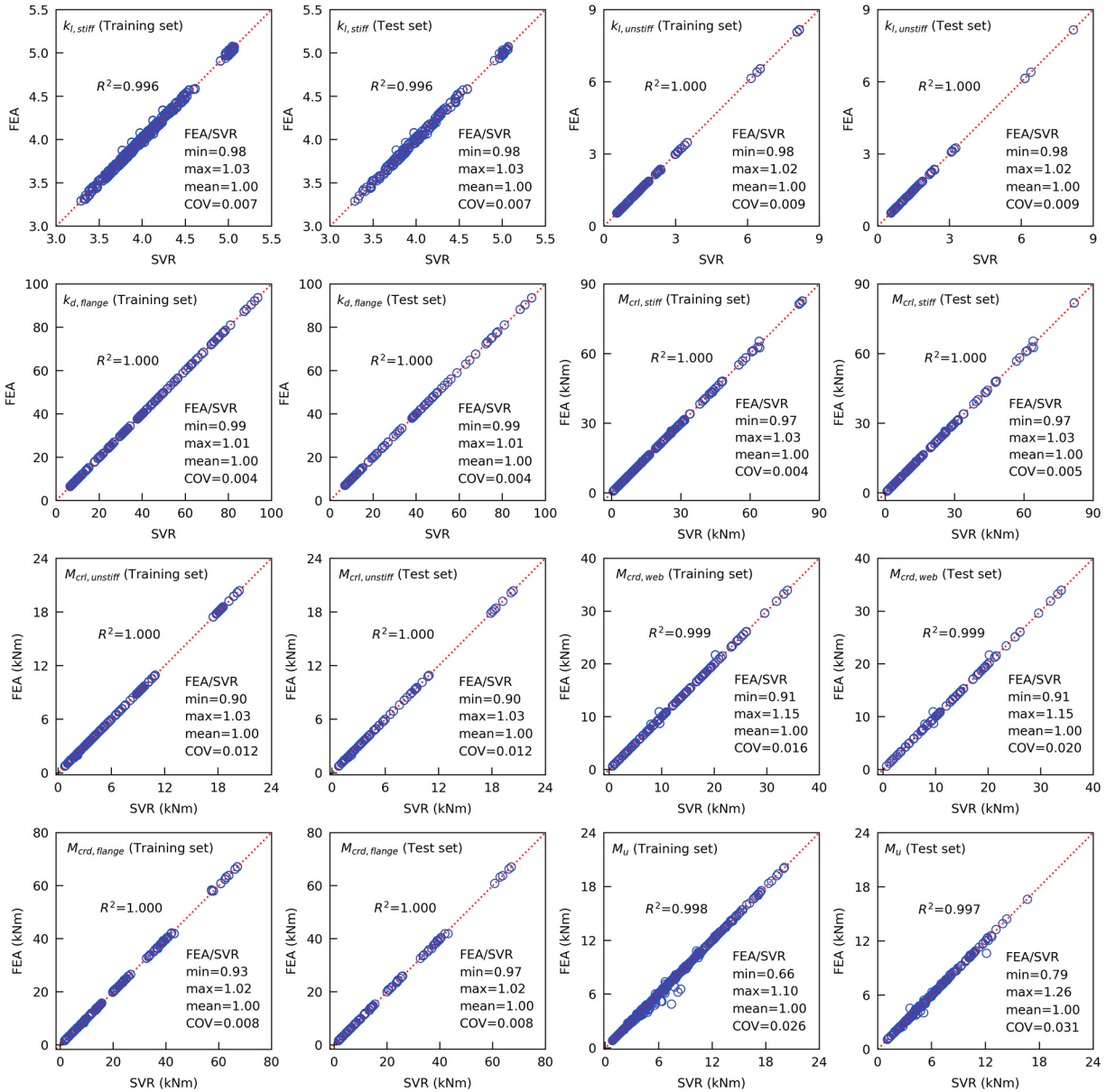

Figure 5: Performance of SVR Models

Table 3: Performance Metrics of SVR for Predicting Buckling Coefficients for Training and Test Sets

Metric	$k_{l,stiff}$		$k_{l,unstiff}$		$k_{d,flange}$	
	Train	Test	Train	Test	Train	Test
RMSE	0.027	0.027	0.009	0.010	0.052	0.062
MAE	0.022	0.022	0.009	0.009	0.047	0.055
MAPE (%)	0.556	0.555	0.835	0.828	0.269	0.290

Table 4: Performance Metrics of SVR for Predicting Moments for Training and Test Sets

Metric	$M_{crl,stiff}$		$M_{crl,unstiff}$		$M_{crd,web}$		$M_{crd,flange}$		M_u	
	Train	Test	Train	Test	Train	Test	Train	Test	Train	Test
RMSE (kNm)	0.142	0.166	0.026	0.026	0.186	0.223	0.173	0.158	0.165	0.164
MAE (kNm)	0.032	0.046	0.008	0.010	0.034	0.055	0.070	0.076	0.045	0.067
MAPE (%)	0.149	0.215	0.331	0.377	0.308	0.494	0.375	0.479	0.904	1.357

It can be concluded from Fig. 5 and Tables 3 and 4 that the developed models demonstrate an excellent accuracy in predicting all considered deck properties and good generalization ability. The differences in the performance metrics for the training and test sets are relatively small, indicating that the models are not prone to overfitting.

6. Feature Importance and Feature Effects

ML models are often criticized and not readily adopted by structural engineers due to their black-box nature, which allows for accurate predictions but cannot be easily understood and explained by humans. Several methods are available and commonly used to explain and interpret ML models (Naser 2021). In the present study, the SHapley Additive exPlanations (SHAP) technique (Lundberg and Lee 2017) was used to evaluate the relative feature importance and feature effects on the deck properties predicted by the developed models. The SHAP method uses the Shapley values from the cooperative game theory. Feature impact on the model predictions is estimated by comparing predictions for models with and without each feature.

The SHAP method reveals feature importance and feature effects for the evaluated ML model. If the model is accurate, the SHAP method results also reflect the actual physical relationships between the features and targets. It was shown in Section 5 that the developed models produce very accurate predictions. Therefore, it can be considered that SHAP relative feature importance and feature effects presented in this section represent the mechanics-based relationships.

Fig. 6 shows SHAP summary plots, which combine feature importance and feature effects for each developed SVR model. Each point on the summary plot represents a dataset sample. The point color corresponds to the feature value ranging from blue for low values to red for high values. Points with the same Shapley values are scattered in the vertical direction. The feature order follows their SHAP importance. Features with higher SHAP values have more significant effects on model predictions.

It should be noted that some dataset features correlated with each other. For example, deeper deck profiles generally had longer spans, wider flanges and pitches, and fewer hats. Heavier profiles had greater bend radii at the steel centerline. Decks with fewer hats had wider pitches. For most profiles, the flat width of the unstiffened deck flanges, w_l, was taken as one-half of the bottom flange flat width, w_{bf}. Therefore, the presented importance and effects of some features on the studied deck properties are driven by other features correlated to the considered ones.
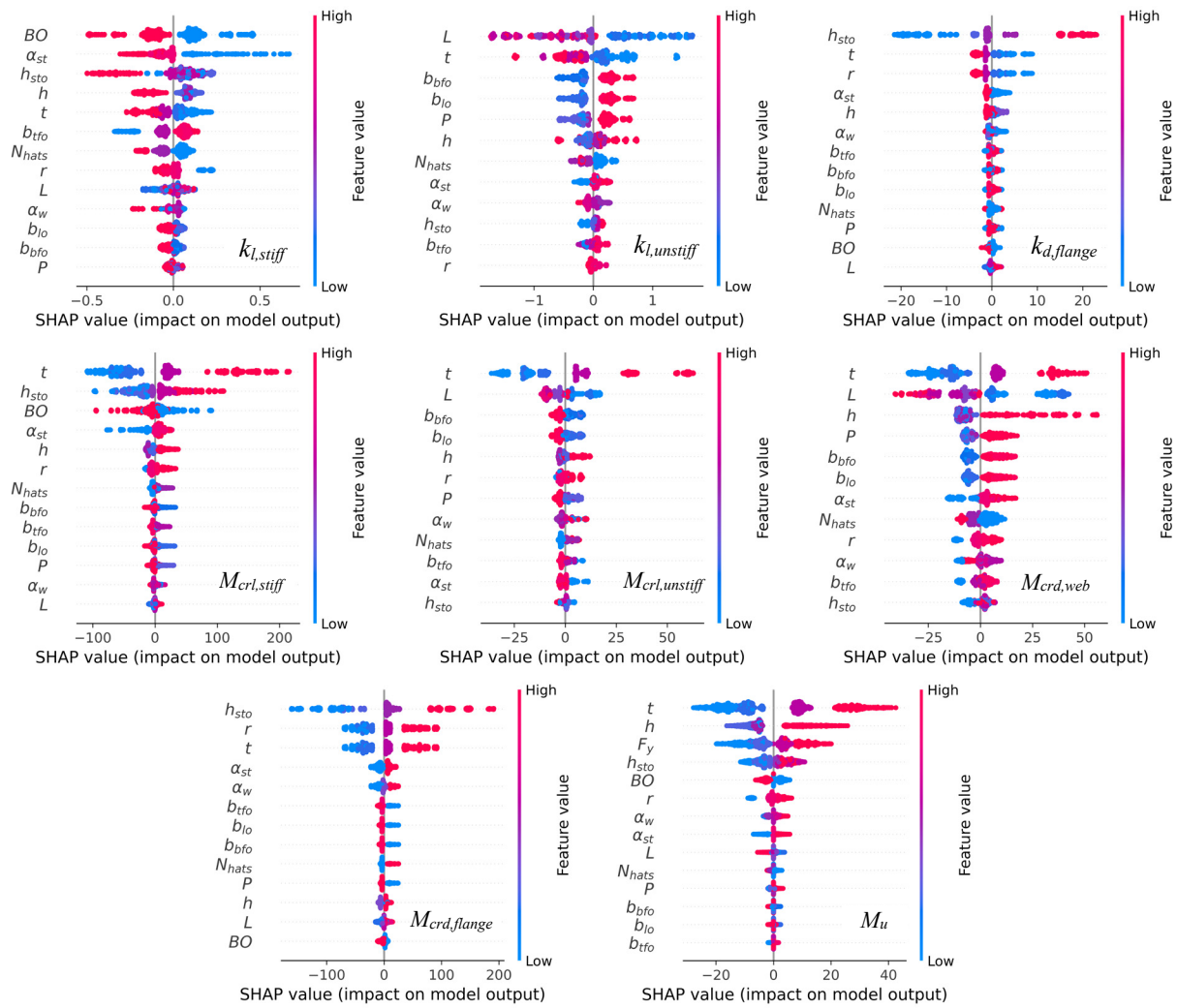
10

Figure 6: SHAP Summary Plots

The deck bending orientation, α_{st}, and h_{sto} had the most significant effects on $k_{l,stiff}$. The positive deck bending (BO=1) produced higher $k_{l,stiff}$ values than negative deck bending (BO=2). These results were driven by the non-symmetric deck sections (1.5B and 3N), for which $k_{l,stiff}$ reduces when the relative neutral axis location increases (Degtyarev 2020a). Greater values of the longitudinal stiffener angle, α_{st}, resulted in higher $k_{l,stiff}$ values, and vice versa. The longitudinal stiffener height, h_{sto}, generally had a similar effect on $k_{l,stiff}$, but the results were somewhat mixed: for some profiles, an increase in h_{sto} resulted in an increase in $k_{l,stiff}$, while the opposite was true for other decks. An increase in deck height, h, resulted in a $k_{l,stiff}$ reduction. This result can be explained as follows. Deck webs in compression are more prone to buckling along with the compression flanges for deeper profiles. The web-flange buckling interaction reduces $k_{l,stiff}$. The $k_{l,stiff}$ values reduced when t increased and increased when the top flange width, b_{tfo}, increased. The effects of h, t, and b_{tfo} on $k_{l,stiff}$ were considerably smaller than the effects of BO, α_{st}, and h_{sto}. The remaining features had even more minor effects on $k_{l,stiff}$.

11

The $k_{l,unstiff}$ values were most affected by the deck span, L, and steel thickness, t. Higher values of L and t produced smaller $k_{l,unstiff}$ values. The effect of L on $k_{l,unstiff}$ can be explained by the aspect ratio reduction when the deck span is shortened and the span length effect on the number of half-waves. However, the latter requires further investigation. b_{bfo} and b_{lo} demonstrated similar effects on $k_{l,unstiff}$, because the flat width of the unstiffened flange was taken as one-half of the bottom flange flat width for most profiles. The $k_{l,unstiff}$ values increased when b_{bfo} and b_{lo} increased. Deck profiles with larger pitches, P, produced higher $k_{l,unstiff}$ values, while the effect of deck height, h, on $k_{l,unstiff}$ was mixed. For most profiles, an increase in h increased $k_{l,unstiff}$, but h affected $k_{l,unstiff}$ oppositely for some decks. The remaining features had minor effects on $k_{l,unstiff}$.

As expected, the longitudinal stiffener height, h_{sto}, had the most significant influence on $k_{d,flange}$. Deeper stiffeners increase the flexural stiffness of flanges, which is reflected in higher $k_{d,flange}$ values. The steel thickness, t, and bend radius, r, showed similar but considerably less significant effects on $k_{d,flange}$. Deck profiles with larger t and r values produced higher $k_{d,flange}$ values. The remaining features affected $k_{d,flange}$ insignificantly.

$M_{crl,stiff}$ was most significantly affected by the steel thickness, t, an increase of which resulted in an $M_{crl,stiff}$ increase. The longitudinal stiffener height, h_{sto}, bending orientation, and longitudinal stiffener angle, α_{st}, followed t in their impacts on $M_{crl,stiff}$, which increased when h_{sto} and α_{st} increased and decreased when the bending orientation changed from normal to inverted. The remaining features had less significant effects on $M_{crl,stiff}$, which increased in most cases when h, r, N_{hats}, and L increased and decreased when b_{bfo}, b_{tfo}, b_{lo}, and P increased.

The effect of the steel thickness, t, on $M_{crl,unstiff}$, was considerably more significant than the effects of other features. $M_{crl,unstiff}$ increased when t increased. The deck span length, L, was the next feature most significantly affecting $M_{crl,unstiff}$, which decreased when L increased. The remaining features had comparable and less significant effects on $M_{crl,unstiff}$. Interestingly, an increase in b_{lo} resulted in $M_{crl,unstiff}$ reduction, whereas deeper deck profiles produced higher $M_{crl,unstiff}$ values.

$M_{crd,web}$ was most significantly affected by t, L, and h. $M_{crd,web}$ increased when t and h increased and reduced when L increased. The remaining features had less significant effects on $M_{crd,web}$. It can be observed from Fig. 6 in particular that profiles with wider unstiffened flanges produced higher $M_{crd,web}$ values.

The longitudinal stiffener height, h_{sto}, and steel thickness, t, had the most significant effects on $M_{crd,flange}$, which increased when h_{sto} and t increased. Fig. 6 also shows the high importance of r for predicting $M_{crd,flange}$, but this result was caused by the correlation between t and r discussed above. The remaining features affected $M_{crd,flange}$ less significantly.

Finally, M_u was most significantly affected by the following features in the descending order: t, h, F_y, and h_{sto}, which increase resulted in a M_u increase, as expected. The bending orientation of non-symmetric deck sections also affected the ultimate moment, which was greater for the normal bending than for the inverted bending. Similar results were obtained previously (Degtyarev 2020a). The remaining features affected M_u less significantly.

Fig. 6 shows that some features had relatively small effects on the studied deck properties. It might be possible to exclude those features from the models without a considerable reduction in the predicting accuracy. However, that was done in this work and will be considered in future studies.

The presented information about the feature importance and feature effects generally aligns with the mechanics-based knowledge, which confirms the abilities of the developed models to capture and reveal the underlying physics from the data used for the model development. At the same time, the new information on the effects of h and t on $k_{l,stiff}$, and L and t on $k_{l,unstiff}$ was obtained.

7. Comparisons

Fig. 7 shows comparisons of the deck properties predicted by the developed SVR models and existing EWM and DSM design provisions (AISI S100-16) with FEA results for the entire dataset.
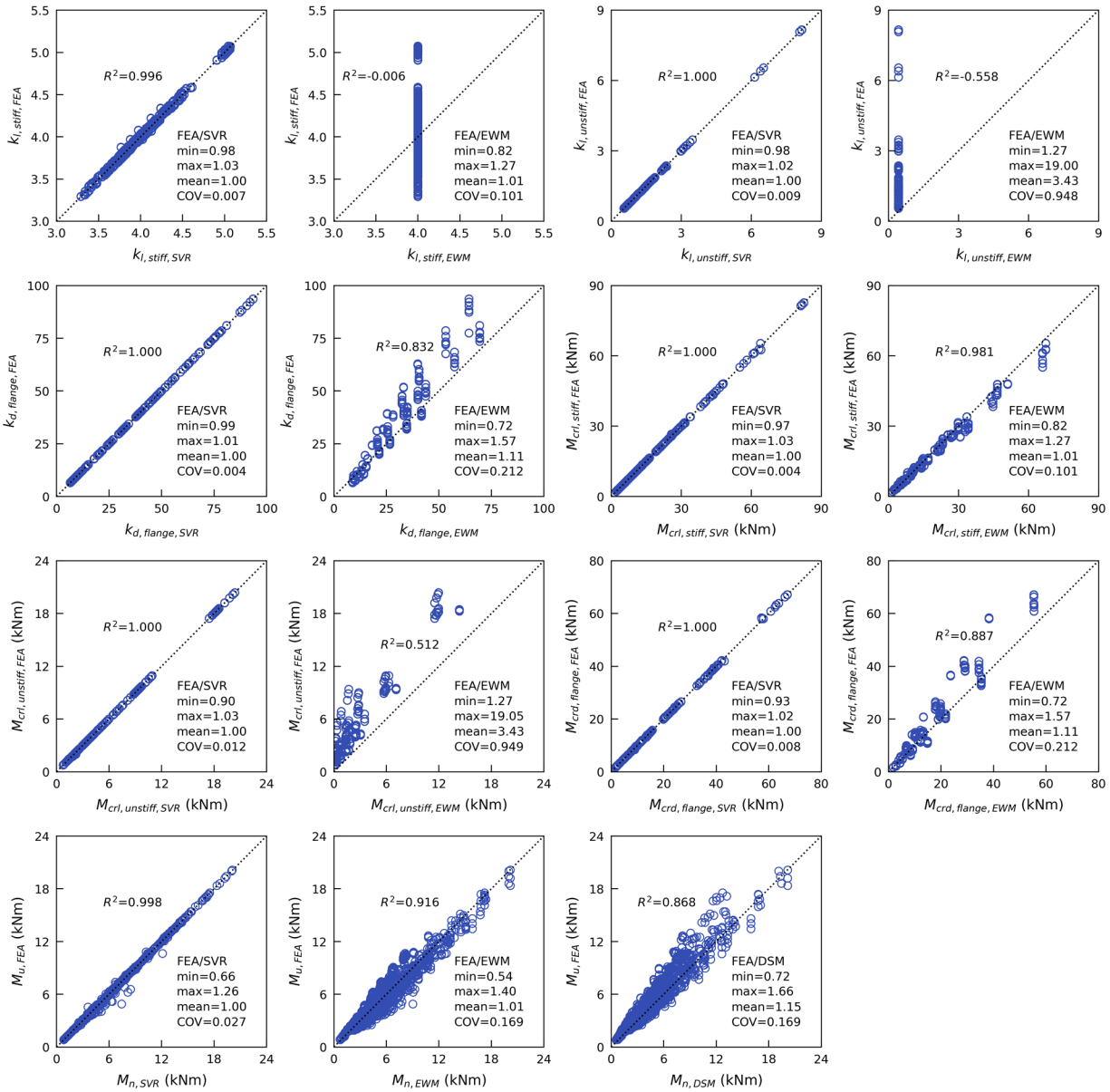

Figure 7: Comparisons of SVR, EWM, and DSM Predictions

13

Prediction performance metrics are given in Fig. 7 and Tables 5 and 6. The elastic buckling properties ($k_{l,stiff}$, $k_{l,unstiff}$, $k_{d,flange}$, $M_{crl,stiff}$, $M_{crl,unstiff}$, and $M_{crd,flange}$) were compared with the EWM only, because in the DSM, they are determined from elastic buckling analyses similar to the ones performed in the present work. Thus, the deck elastic buckling properties according to the DSM are identical to those from FEA obtained in this study. Comparisons for $k_{d,web}$ and $M_{crd,web}$ are not presented because the EWM cannot predict them.

Table 5: Performance Metrics of SVR and EWM for Predicting Buckling Coefficients

Metric	$k_{l,stiff}$		$k_{l,unstiff}$		$k_{d,flange}$	
	SVR	EWM	SVR	EWM	SVR	EWM
RMSE	0.027	0.409	0.010	1.743	0.054	9.216
MAE	0.022	0.308	0.009	1.044	0.048	6.507
MAPE (%)	0.556	7.488	0.833	56.955	0.273	18.559

Table 6: Performance Metrics of SVR, EWM, and DSM for Predicting Moments

Metric	$M_{crl,stiff}$		$M_{crl,unstiff}$		$M_{crd,flange}$		M_u		
	SVR	EWM	SVR	EWM	SVR	EWM	SVR	EWM	DSM
RMSE (kNm)	0.147	2.170	0.026	3.529	0.170	5.064	0.165	0.969	1.212
MAE (kNm)	0.034	1.205	0.009	2.950	0.071	3.303	0.050	0.760	0.898
MAPE (%)	0.162	7.488	0.341	56.96	0.396	18.559	0.995	14.380	15.688

The presented information demonstrates the superior performance of the developed SVR models for predicting the steel deck buckling coefficients, buckling moments, and ultimate moment compared with the existing design methods.

8. Web Application
A web application to predict deck properties in bending by the developed SVR models was created in Streamlit (https://streamlit.io). Fig. 8 shows the graphical user interface of the web application.
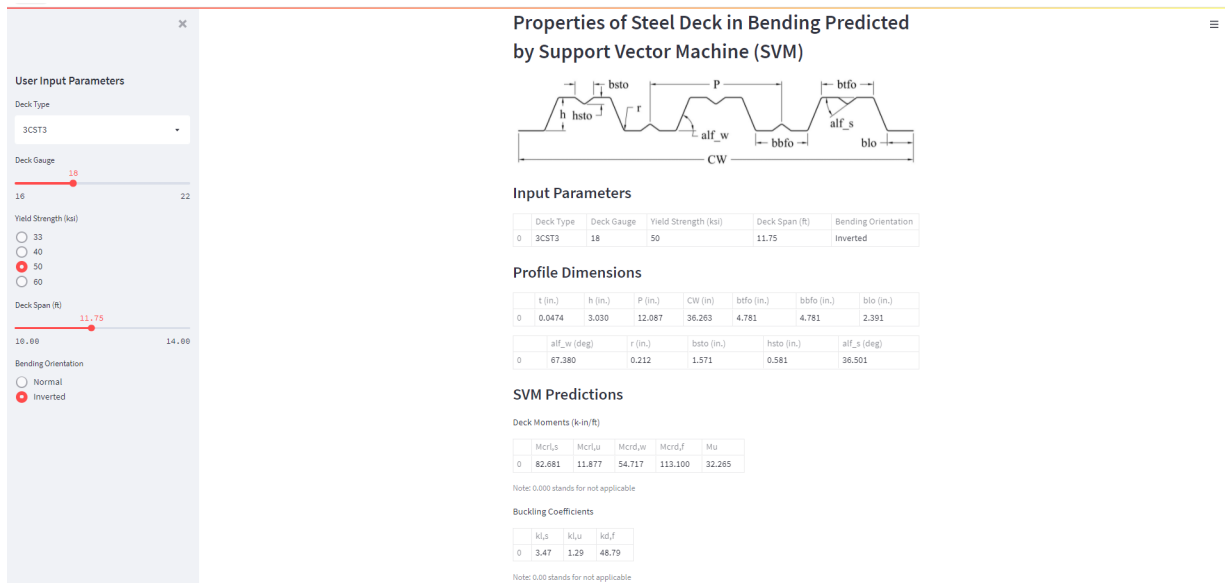

Figure 8: Graphical User Interface of the Developed Web Application

The application predicts the $k_{l,stiff}$, $k_{l,unstiff}$, $k_{d,flange}$, $M_{crl,stiff}$, $M_{crl,unstiff}$, $M_{crd,flange}$, and M_u values based on the following parameters specified by the user: deck type, deck gauge, yield strength, deck span, and bending orientation. The application's source code is available in Degtyarev (2021d). It allows for running the application on a local machine. The application has also been deployed to the cloud. It can be opened and run in any browser on any device, including mobile, at https://steel-deck-bending.herokuapp.com/.

9. Conclusions and Future Work

The paper presented Support Vector Machine regression (SVR) models for predicting the following properties of steel deck profiles commonly used in North America: plate buckling coefficients of stiffened flanges, plate buckling coefficients of unstiffened flanges, plate buckling coefficient for distortional buckling of deck flanges with a longitudinal stiffener, local elastic buckling moment of stiffened flanges, local elastic buckling moment of unstiffened flanges, distortional elastic buckling moment of a web-edge flange junction, distortional elastic buckling moment of a flange-stiffener junction, and ultimate moment. The models were trained, validated, and tested using a large finite element analysis results dataset. The developed models demonstrated a good generalization ability and excellent prediction accuracy, which exceeded the accuracy of the existing design methods.

The SVR models were interpreted by evaluating feature importance and feature effects on the studied deck properties with the SHapley Additive exPlanations (SHAP) method. The obtained feature importance and feature effects aligned well with the mechanics-based knowledge, confirming the abilities of the developed models to capture and reveal the underlying physics from the data used for the model development.

For non-symmetric deck cross-sections, the effects of the flange width ratio on the plate buckling coefficients of stiffened flanges, the local elastic buckling moment of stiffened flanges, and the ultimate moment presented previously were confirmed. The new information on the effects of deck height and steel thickness on the plate buckling coefficients of stiffened flanges and span length and steel thickness on the plate buckling coefficients of unstiffened flanges was obtained.

A web application for predicting the studied deck properties in bending by the developed SVR models was created and deployed to the cloud at https://steel-deck-bending.herokuapp.com/. It can be opened and run in any browser on any device, including mobile. The application's source code is available on GitHub, which allows for running the application locally.

The presented study demonstrates a high potential of machine learning methods for predicting buckling and ultimate loads of cold-formed steel decks. Considering the magnitude of different deck profiles available worldwide, future work should concentrate on expanding the database to decks of different shapes and dimensions. Machine learning models based on other commonly used regression algorithms should also be studied to determine the algorithm with the highest accuracy and the best generalization.

References

Adeli, H., Karim, A. (1997). "Neural network model for optimization of cold-formed steel beams." Journal of Structural Engineering, 123(11), 1535-1543.

AISI S100-16. (2020). "North American Specification for the Design of Cold-formed Steel Structural Members," 2016 Ed. with Supplement 2. American Iron and Steel Institute, Washington, DC.

Ali, A.A. (2017). "Neural network modeling for rotational capacity of cold-formed purlin steel sections." International Journal of Civil Engineering and Technology (IJCIET), 8(12), 362-372.

ANSYS Mechanical APDL, Release 19.2.

AS/NZS 4600:2018. (2018). "Cold-formed steel structures." Standards Australia/Standards New Zealand, Sydney, Australia/Wellington, New Zealand.

Çevik, A., Kurtoğlu, A.E., Bilgehan, M., Gülşan, M.E., Albegmprli, H.M. (2015). "Support vector machines in structural engineering: a review." Journal of Civil Engineering and Management, 21(3), 261-281.

Cortes, C., Vapnik, V. (1995). "Support-vector networks." Machine learning, 20(3), 273-297.

Claesen, M., Simm, J., Popovic, D., Moreau, Y., De Moor, B. (2014). "Easy hyperparameter search using optunity." *arXiv preprint arXiv*:1412.1114.

Clerc, M., Kennedy, J. (2002). "The particle swarm-explosion, stability, and convergence in a multidimensional complex space." IEEE transactions on Evolutionary Computation, 6(1), 58-73.

D'Aniello, M., Güneyisi, E.M., Landolfo, R., and Mermerdaş, K. (2014). "Analytical prediction of available rotation capacity of cold-formed rectangular and square hollow section beams." Thin-Walled Structures, 77, 141-152.

Degtyarev, V.V. (2020a). "Computational study of elastic buckling and post-buckling strength of steel decks in bending." Proceedings of the Annual Stability Conference. Structural Stability Research Council (SSRC), Atlanta, Georgia.

Degtyarev, V.V. (2020b). "Concentrated load distribution in corrugated steel decks: A parametric finite element study." Engineering Structures, 206, 110158.

Degtyarev, V.V. (2020c). "Finite element modeling of cold-formed steel deck in bending." Magazine of Civil Engineering, 94(2), 129-144

Degtyarev, V.V. (2020d). "Flexural strength of steel decks with square and rectangular holes: Numerical studies." Journal of Constructional Steel Research, 172, 106241.

Degtyarev, V.V. (2021a), "Elastic buckling and post-buckling strength of CFS decks in bending: FE simulation results," Mendeley Data, V3, doi: 10.17632/3km4b3sfcw.3.

Degtyarev, V.V. (2021b). "Neural networks for predicting shear strength of CFS channels with slotted webs." Journal of Constructional Steel Research, 177, 106443.

Degtyarev, V.V. (2021c). "Predicting shear strength of CFS channels with slotted webs by machine learning models." Architecture, Structures and Construction, 1-18.

Degtyarev, V.V. (2021d). "Web application to predict deck properties in bending by SVR models." https://github.com/vitdegtyarev/Steel_Deck-Streamlit.

Degtyarev, V.V., and Naser, M.Z. (2021). "Boosting machines for predicting shear strength of CFS channels with staggered web perforations." Structures, 34, 3391-3403.

Dudenbostel, R.K., and Sputo. T. (2016). "Application of the Direct Strength Method to steel deck." Proceedings of Wei-Wen Yu International Specialty Conference on Cold-Formed Steel Structures, Baltimore, MD, 665-679.

El-Kassas, E.M.A., Mackie, R.I., and El-Sheikh, A.I. (2002). "Using neural networks to predict the design load of cold-formed steel compression members." Advances in Engineering Software, 33(7-10), 713-719.

EN 1993-1-5:2006. (2006). "Eurocode 3 - Design of steel structures - Part 1-5: Plated structural elements." European Committee for Standardization, Brussels, Belgium.

Gardner, L. and Yun, X. (2018). "Description of stress-strain curves for cold-formed steels." Construction and Building Materials, 189, 527-538.

Fang, Z., Roy, K., Chen, B., Sham, C.W., Hajirasouliha, I., and Lim, J.B. (2021c). "Deep learning-based procedure for structural design of cold-formed steel channel sections with edge-stiffened and un-stiffened holes under axial compression." Thin-Walled Structures, 166, 108076.

Fang, Z., Roy, K., Ma, Q., Uzzaman, A., and Lim, J.B. (2021a). "Application of deep learning method in web crippling strength prediction of cold-formed stainless steel channel sections under end-two-flange loading." Structures, 33, 2903-2942.

Fang, Z., Roy, K., Mares, J., Sham, C.W., Chen, B., and Lim, J.B. (2021b). "Deep learning-based axial capacity prediction for cold-formed steel channel sections using Deep Belief Network." Structures, 33, 2792-2802.

Guzelbey, I.H., Cevik, A., and Erklig, A. (2006). "Prediction of web crippling strength of cold-formed steel sheetings using neural networks." Journal of Constructional Steel Research, 62(10), 962-973.

Karim, A., and Adeli, H. (1999). "Global optimum design of cold-formed steel hat-shape beams." Thin-Walled Structures, 35(4), 275-288.

Lee, J., Kim, S.M., and Park, H.S. (2006). "Optimum design of cold-formed steel columns by using micro genetic algorithms." Thin-Walled Structures, 44(9), 952-960.

Lundberg, S. M., Lee, S.-I. (2017). "A unified approach to interpreting model predictions." Advances in neural information processing systems 30, I. Guyon, U. V. Luxburg, S. Bengio, H. Wallach, R. Fergus, S. Vishwanathan, and R. Garnett, eds., Curran Associates, Inc., 4765-4774.

Naser, M.Z. (2021). "An engineer's guide to explainable artificial intelligence and interpretable machine learning: Navigating causality, forced goodness, and the false perception of inference." Automation in Construction, 129,103821.

Naser, M.Z., and Alavi, A.H. (2021). "Error metrics and performance fitness indicators for artificial intelligence and machine learning in engineering and sciences," Architecture, Structures and Construction, https://doi.org/10.1007/s44150-021-00015-8.

Naser, M.Z., Kodur, V., Thai, H.T., Hawileh, R., Abdalla, J., and Degtyarev, V.V. (2021). "StructuresNet and FireNet: Benchmarking databases and machine learning algorithms in structural and fire engineering domains." Journal of Building Engineering, 44, 102977.

Oey, O., Papangelis, J. (2020). "Nonlinear Analysis of Cold-Formed Channels Bent about the Minor Axis." Proceedings of the Cold-Formed Steel Research Consortium Colloquium, 20-22 October 2020, https://jscholarship.library.jhu.edu/handle/1774.2/63148.

Pala, M. (2006). "A new formulation for distortional buckling stress in cold-formed steel members." Journal of Constructional Steel Research, 62(7), 716-722.

Pala, M. (2008). "Genetic programming-based formulation for distortional buckling stress of cold-formed steel members." Journal of Constructional Steel Research, 64(12), 1495-1504.

Pala, M., Caglar, N. (2007). "A parametric study for distortional buckling stress on cold-formed steel using a neural network." Journal of Constructional Steel Research, 63(5), 686-691.

Pedregosa, F., Varoquaux, G., Gramfort, A., Michel, V., Thirion, B., Grisel, O., Blondel, M., Prettenhofer, P., Weiss, R., Dubourg, V., Vanderplas, J. (2011). "Scikit-learn: Machine learning in Python." The Journal of Machine Learning Research, 12, 2825-2830.

Pham, S.H. (2018). "Design of cold-formed steel beams with holes and transverse stiffeners in shear." Ph.D. Thesis, The University of Sydney. Sydney, Australia.

Raebel, C., Gwozdz, D. (2018). "Comparison of experimental and numerical results for flexural capacity of light-gage steel roof deck." Proceedings of Wei-Wen Yu International Specialty Conference on Cold-Formed Steel Structures, St. Louis, MO, 55-67.

Raebel, C.H., Schultz, J.A., and Whitsell, B. (2020). "Experimental investigation into acceptable design methods for cold-formed metal deck." Journal of Constructional Steel Research, 172, 106176.

Salehi, H., Burgueño, R., (2018). "Emerging artificial intelligence methods in structural engineering." Engineering Structures, 171, 170–189.

Schafer, B.W. (2008). "Review: The Direct Strength Method of cold-formed steel member design." Journal of Constructional Steel Research, 64, 766-778.

Schafer, B.W. (2019). "Advances in the Direct Strength Method of cold-formed steel design." Thin-Walled Structures, 140, 533-541.

Schafer, B.W., Peköz, T. (1998). "Direct Strength prediction of cold-formed steel members using numerical elastic buckling solutions." Proceedings of Fourteenth International Specialty Conference on Cold-Formed Steel Structures, St. Louis, MO, 69-76.

Sirca Jr., G.F., Adeli, H. (2001). "Neural network model for uplift load capacity of metal roof panels." Journal of Structural Engineering, 127(11), 1276-1285.

Smola, A.J., Schölkopf, B. (2004). "A tutorial on support vector regression." Statistics and computing, 14(3), 199-222.

Sun, H., Burton, H.V., Huang, H. (2021). "Machine learning applications for building structural design and performance assessment: state-of-the-art review." Journal of Building Engineering, 33, 101816.

Timoshenko, S.P., Gere, J.M. (1963). "Theory of elastic stability." 2nd International Student Ed., *McGraw-Hill*, Singapore.

Taheri, E., Esgandarzadeh Fard, S., Zandi, Y., Samali, B. (2021). "Experimental and numerical investigation of an innovative method for strengthening cold-formed steel profiles in bending throughout finite element modeling and application of neural network based on feature selection method." Applied Sciences, 11(11), 5242.

Vapnik, V. (1995). "The nature of statistical learning theory." *Springer*, New York.

Vapnik, V., Golowich, S.E., Smola, A. (1997). "Support vector method for function approximation, regression estimation, and signal processing." Advances in neural information processing systems, 281-287.

von Karman, T., Sechler, E.E., Donnell, L.H. (1932). "The strength of thin plates in compression." Transactions ASME, 54(APM 54-5), 53-57.

Winter, G. (1947). "Strength of thin steel compression flanges." Transactions of ASCE, 112(1), 527-554.

Yu, C., Lokie, T. (2006). "Effective width method based design for distortional buckling." Proceedings of Eighteenth International Specialty Conference on Cold-Formed Steel Structures, Orlando, FL, 105-118.